HETEROCYCLES, Vol. 103, No. 2, 2021, pp. 952 - 964. © 2021 The Japan Institute of Heterocyclic Chemistry
Received, 30th November, 2020, Accepted, 12th January, 2021, Published online, 22nd February, 2021
DOI: 10.3987/COM-20-S(K)64

A THEORETICAL STUDY OF PRODUCT SELECTIVITY IN RHODIUM-CATALYZED OXIDATIVE COUPLING REACTION CAUSED BY THE SOLVATION EFFECT

Masahiro Higashi,[1,2]* Naoto Shibata,[1] Suguru Takeno,[1] Tetsuya Satoh,[3] Masahiro Miura,[4] and Hirofumi Sato[1,2,5]*

[1]Department of Molecular Engineering, Graduate School of Engineering, Kyoto University, Nishikyo-ku, Kyoto 615-8510, Japan. [2]Elements Strategy Initiative for Catalysts and Batteries (ESICB), Kyoto University, Kyoto 615-8520, Japan. [3]Department of Chemistry, Graduate School of Science, Osaka City University, 3-3-138 Sugimoto, Sumiyoshi-ku, Osaka 558-8585, Japan. [4]Department of Applied Chemistry, Graduate School of Engineering, Osaka University, Suita, Osaka, 565-0871, Japan. [5]Fukui Institute for Fundamental Chemistry, Kyoto University, Kyoto 606-8103, Japan.
E-mail: higashi@moleng.kyoto-u.ac.jp, hirofumi@moleng.kyoto-u.ac.jp

Abstract – Solvation effects in the direct oxidative coupling of 1-phenylpyrazole with alkynes in the presence of rhodium catalyst was theoretically studied by means of the reference interaction site model self-consistent field with spatial electron density distribution (RISM-SCF-SEDD) method, which provides both of quantum chemical and statistical mechanical information on the solvation system. This reaction gives naphthalene and quinoline derivatives whose yields depend on the solvent environment. The computational results showed that the path for the naphthalene derivative is exothermic independently of solvent environment. On the other hand, the reaction energy of the reductive elimination for the quinoline derivative is considerably affected by solvation and endothermic in *N*,*N*-dimethylformamide (DMF) solution, indicating that the reaction is not preferable in DMF solution. The detailed analysis of solvation free energy and solvation structure are also reported.

INTRODUCTION

Syntheses of polycyclic aromatic and heteroaromatic compounds attract great attentions because of their potential use of π-conjugated functional materials such as organic semiconductor and luminescent materials.[1,2] There are several ways in synthesizing fused aromatic ring. Recently, an efficient and easily tunable synthesis of the transition-metal-catalyzed homologation by the coupling of a given aromatic substrate with two alkyne molecules has been developed by Miura group.[3,4] One of the significantly interesting features of this reaction is that the product is controlled by solvent.[5] A quinoline derivative is obtained only in *o*-xylene solution while a naphthalene derivative is produced either in *o*-xylene and *N*, *N*-dimethylformamide (DMF) solution. At the present, this reaction is assumed to proceed in the following steps[3–10] (Scheme 1): (i) C–H bond cleavage by rhodium catalyst; (ii) insertion of alkyne substrates to afford a seven-membered ring compound (B); (iii) subsequent C–H bond activation after cleavage of Rh–N coordination; In this step, two paths (path I and II) are conceivable with respect to activation of different C–H bond. Passing through the elimination of rhodium catalyst, two different products are obtained depending on solvent environment as mentioned above. A question arises here is how the solvent controls the product selectivity, especially at the molecular level. Since DMF solvent is polar and capable to directly coordinate the rhodium, which is different from *o*-xylene, a detailed solvation structure may be required to correctly understand the origin of the selectivity.

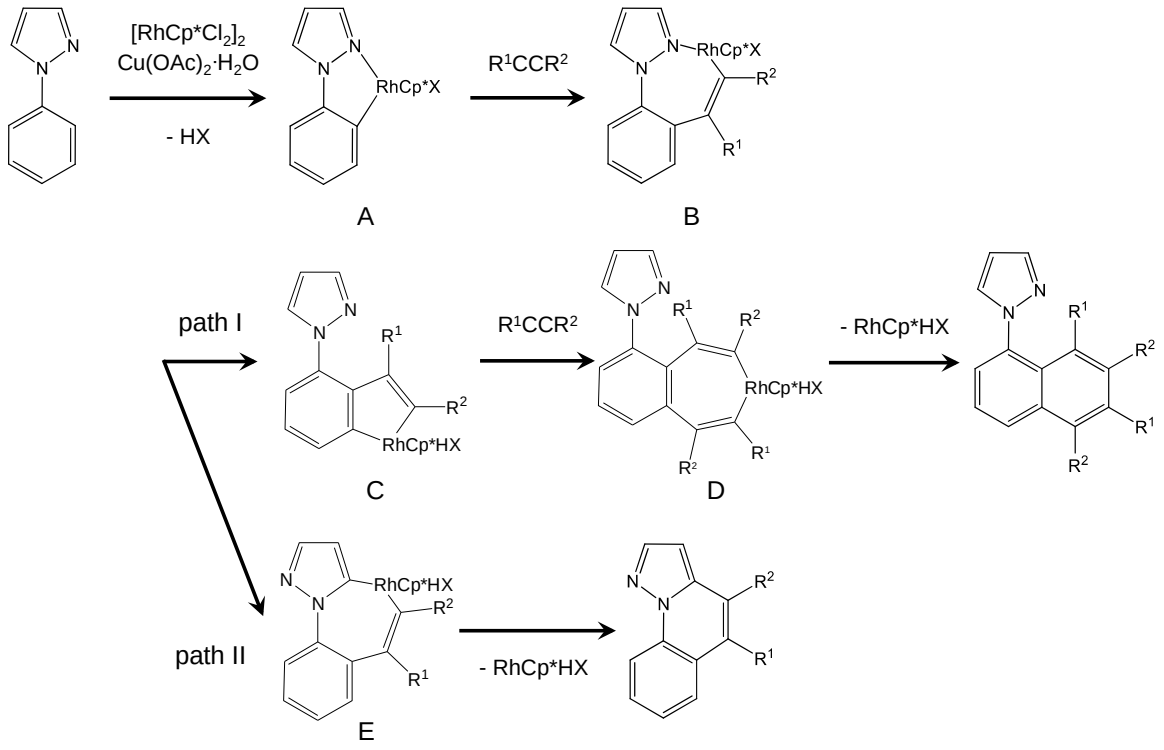

Scheme 1

The present paper investigates the solvent effect on this selectivity using the reference interaction site model self-consistent field (RISM-SCF) with spatial electron density distribution (SEDD) method.[11–13] The oxidative coupling of 1-phenylpyrazole and acetylene with rhodium catalysis was employed as the target system. To reduce computational cost, we adopted [$RhCpCl_2$] as rhodium catalyst instead of [$RhCp^*Cl_2$]. We would like to emphasize that many experimental studies have been performed in solution phase, but the solvent effect, especially on the transition metal complex, is not sufficiently understood. This is because a hybrid type computation such as a combined quantum mechanical and molecular mechanical (QM/MM) method is generally too time-consuming to treat a large system with reliable accuracy and adequate sampling. The RISM-SCF is a hybrid method of two ab initio methods in theoretical chemistry: one is reference interaction site model (RISM),[14,15] and the other is ab initio QM theory. The method determines the electronic structure and solvent distribution around a solute molecule in a self-consistent manner. It is regarded as an alternative to QM/MM method, however, thanks to the analytical nature of RISM, the electronic structure described in high-level quantum chemical method is obtained together with information of solvation structure at the molecular level. The RISM-SCF has been successfully applied to a wide range of chemical phenomenon in solution phase[16] including organometallic reaction,[17] chemical reaction in ionic liquid,[18] etc. Although the polarizable continuum model (PCM)[19] is the most popular and powerful method on electronic structure study of solvated molecule, the present RISM-SCF-SEDD method could be an alternative to clarify the reaction mechanism at the molecular level.[17,20,21] In the present study, the reaction profile in the gas phase is regarded as that in non-polar *o*-xylene solution and compared with that in polar DMF solution calculated with the RISM-SCF-SEDD method (see EXPERIMENTAL section for details).

RESULTS AND DISCUSSION

The target reaction is initiated by the first C-H cleavage as shown in Scheme 1. The first two steps have been intensively studied. For example, Davies et al. have reported that Cl^- dissociation is a key of the activation, and electrophilic C-H activation is favored in [Ir(DMBA-H)(OAc)Cp*]$^+$ system with little dependence on the metal center.[6] The experimental studies by Jones et al. also indicate that the alkyne insertion could readily occur with Cl^- dissociation.[7–9] Therefore, the seven-membered rhodacycle intermediate **1** shown in Figure 1 was adopted as the starting material of the present computation.

Path to generate naphthylpyrazole (path I)

The first step is a cleavage of Rh-N in **1**, which takes place through transition state **TS**$_{1–2}$ to afford **2**. The acetate group bidentately coordinates to the rhodium center, and also interacts with hydrogen of the phenyl group in **2**. Next, proton transfer takes place through the six-membered transition state structure

TS$_{2–3}$ to afford **3**, in which a five-membered ring is obtained due to a bond formation between Rh and phenyl group. The acetic acid also coordinates to the rhodium. As the reaction proceeds from **1** to **3**, the distance between rhodium and acetate oxygen is gradually increased from 2.07 to 2.17 Å, suggesting weakening of the metal-acetate interaction. Then an acetylene is easily inserted into Rh-C bond to afford **4**. We could not find the transition state from **3** to **4**, probably due to the great stabilization of **4** formation. The final step is reductive elimination of rhodium catalysis from this remarkably stable **4**. A naphthylpyrazole – rhodium complex **5** is obtained through transition state **TS$_{4–5}$**. This complex is finally separated into naphthylpyrazole **6** and [CpRh(AcOH)].

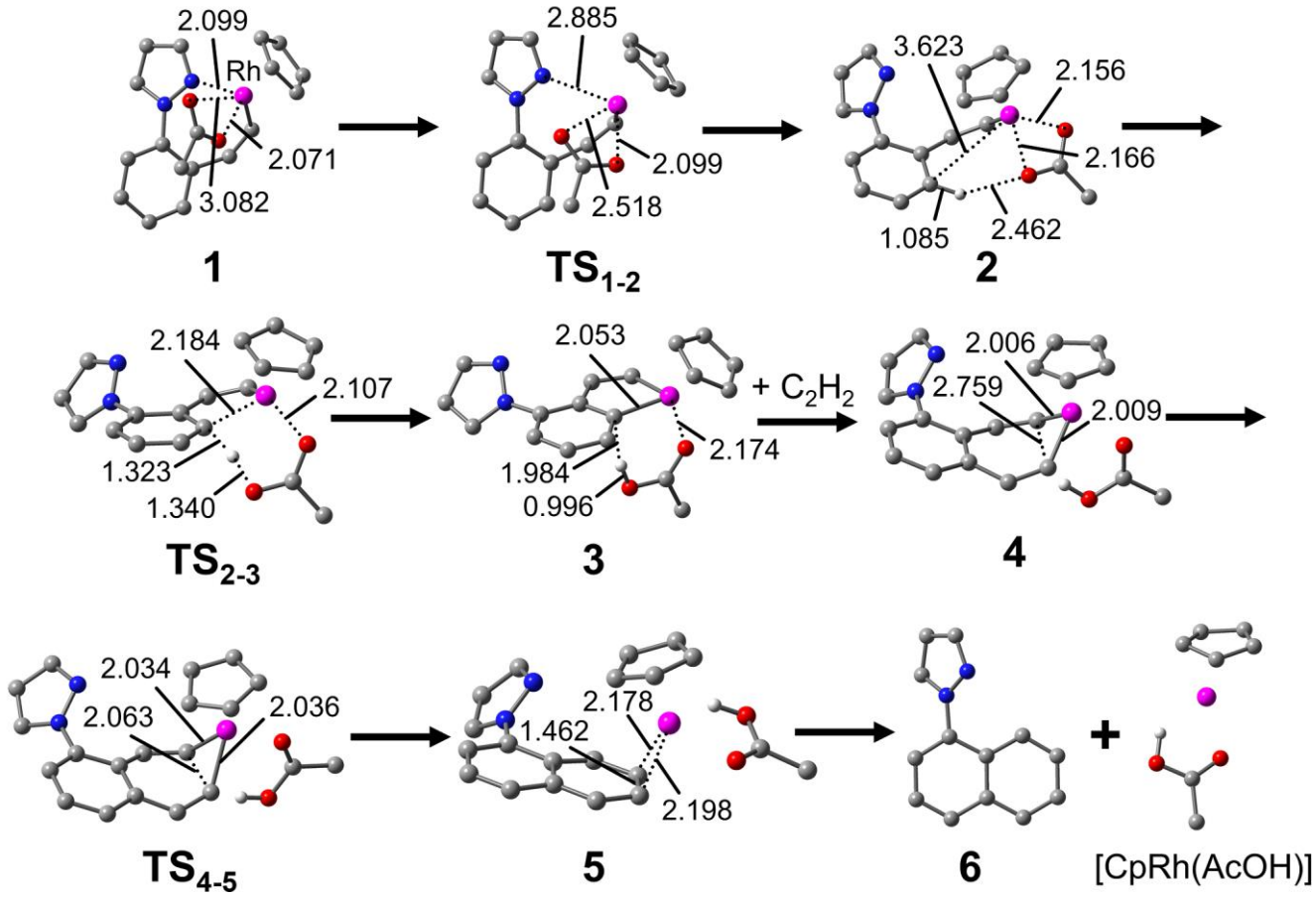

Figure 1. Geometry changes in the reaction of path I. Only important hydrogen atoms are shown for simplicity. Distances are given in Å.

The free energy changes along the reaction of path I is plotted in Figure 2 (left). In the gas phase, the activation free energies of the cleavage of Rh-N (17.7 kcal/mol) and H transfer (19.2 kcal/mol) are not different from each other. The latter is very similar to that of the electrophilic C-H activation computed in the Ir case (16.0 kcal/mol).[6] As mentioned above, **4** is remarkably stable (−18.0 kcal/mol in free energy), and thus the subsequent elimination readily occurs with the modest barrier. The large stabilization

energies of **4** is probably due to the release of distortion energy of the five-membered ring in **3**. Several isomers of **4**, **TS**$_{4-5}$ and **5** were found with respect to the orientation of the acetic acid moiety, but the reaction profile shown here is essentially the same among them. It is noted that the potential energy profile calculated with the B3LYP functional is similar to that with the second-order Møller–Plesset perturbation theory (MP2). For example, the activation barrier of **TS**$_{1-2}$ with respect to **1** and stabilization energy of **4** with respect to **3** calculated with B3LYP are 19.1 and −44.4 kcal/mol whereas those with MP2 are 22.7 and −43.3 kcal/mol. These results indicate the validity of our calculation.

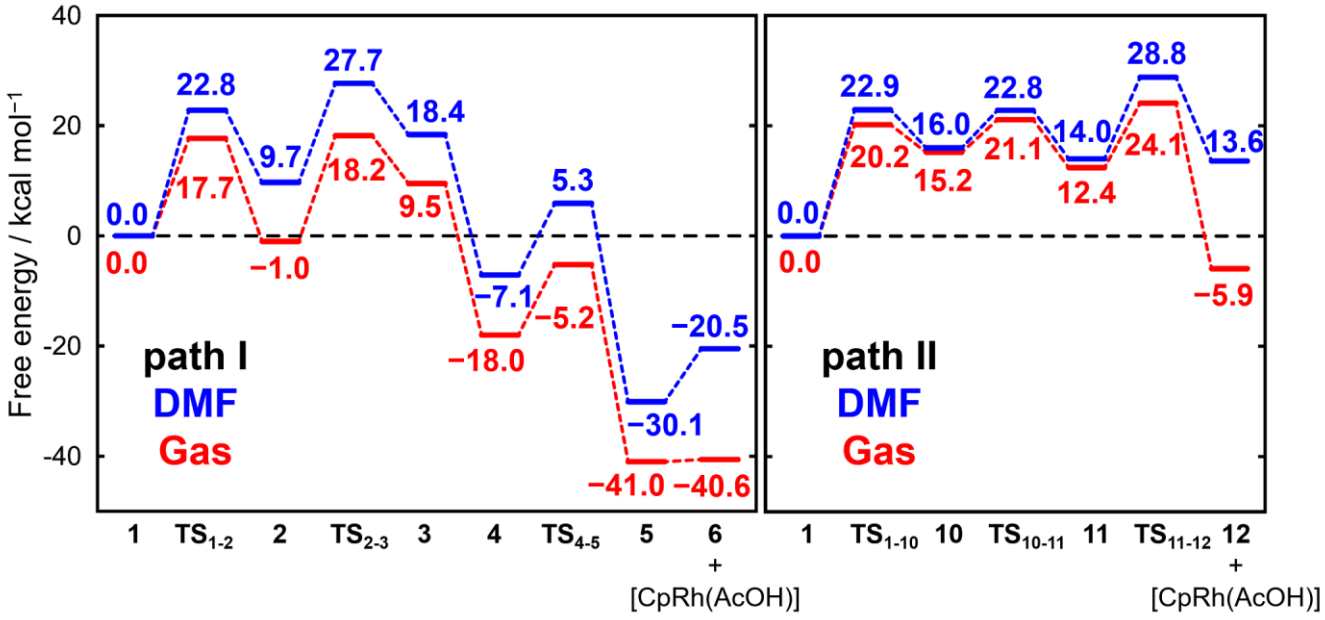

Figure 2. Free energy changes in the gas phase (red line) and in DMF solution (blue line) along the reactions of path I (left) and path II (right).

The reaction profile of path I in DMF solution is not significantly different from the gas phase one. The activation barrier of the cleavage of Rh-N bond is slightly higher (22.8 kcal/mol) than that in the gas phase, but the activation energies for the following two steps, **TS**$_{2-3}$ and **TS**$_{4-5}$, (18.0 and 12.4 kcal/mol, respectively) are almost the same as to those in the gas phase (19.2 and 12.9 kcal/mol). The reason is simply attributed to relatively strong stabilization of **1** due to solvation compared to the other intermediates. It is important that the final state, **6** + [CpRh(AcOH)], is very stable both in the gas phase and in DMF solution (−40.6 and −20.5 kcal/mol).[22] One might consider the possibility of another path from **3**. If the generated AcOH is dissociated from the rhodium complex before the insertion, **7** would be produced (data not shown). However, **7** is unstable about 10 kcal/mol compared to **3**. A concerted path, in which the acetic acid dissociation and the acetylene insertion simultaneously occur, was also found. However, the barrier is further higher (more than 20 kcal/mol) than the stepwise path mentioned above. Another path is the dissociation of AcOH after the insertion of acetylene. But the relative free energy of a

rhodacycle intermediate **8** is about −14 kcal/mol, suggesting that the recombination with AcOH should occur to reproduce **4**. Therefore, the reaction does proceed essentially the aforementioned path. In summary, the naphthalene derivative **6** is generated in both *o*-xylene and DMF solutions through the exothermic reaction.

Path to generate pyrazoloquinoline (path II)

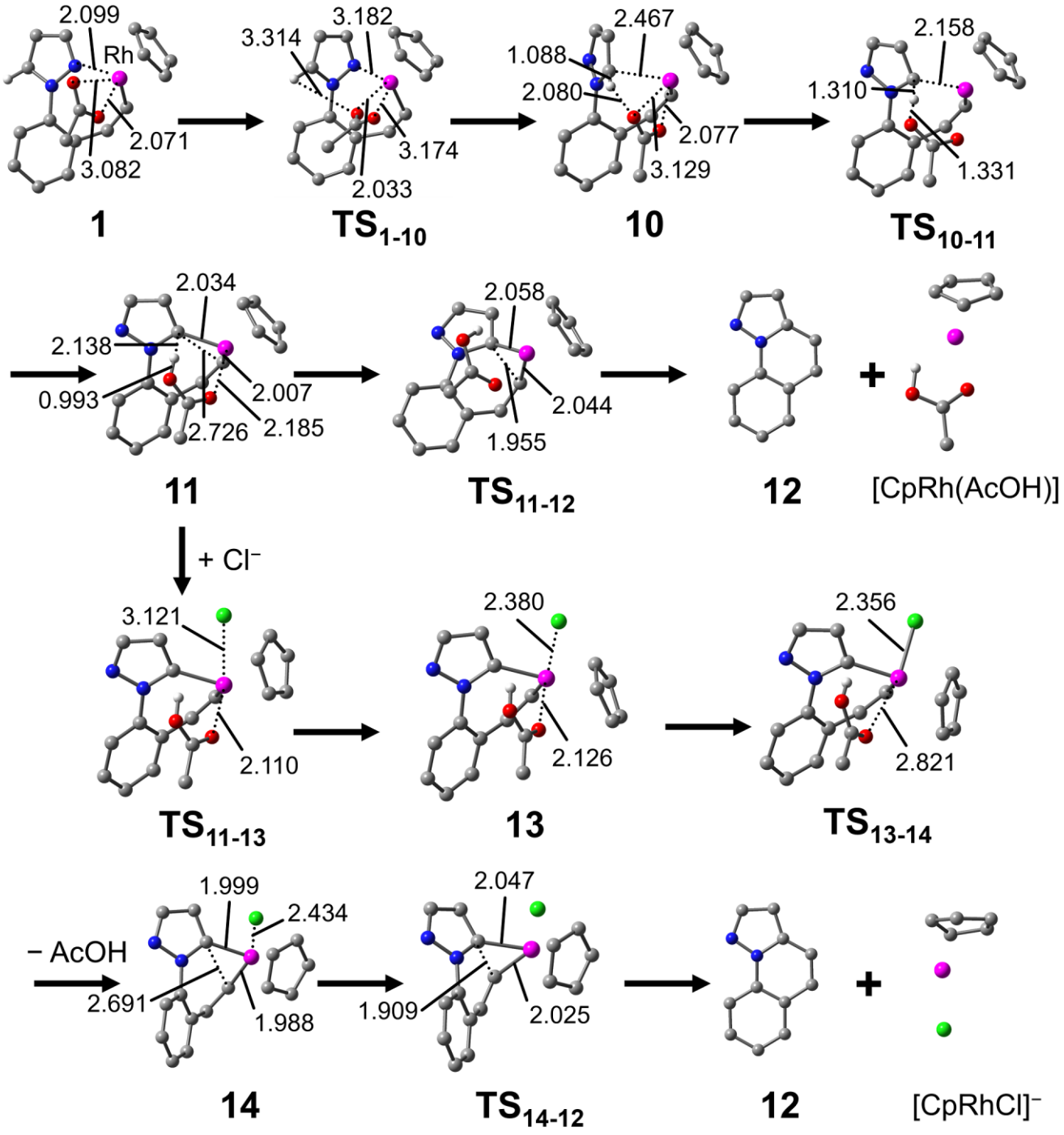

Figure 3. Geometry changes in the reaction of path II. Only important hydrogen atoms are shown for simplicity. Distances are given in Å.

The reaction of path II begins from the seven-membered rhodacycle intermediate **1** (Figure 3). First, the pyrazole ring is significantly rotated with respect to the phenyl group from **1** through transition state **TS$_{1–10}$** to **10**. Dihedral angles of rotating N-N-C-C are −57.8, 49.9, and 80.6 for **1**, **TS$_{1–10}$** and **10**, respectively. At the same time, Rh-N bond is broken and is gradually lengthened; 2.10, 3.18 and 3.89 Å for **1**, **TS$_{1–10}$** and **10**, respectively. The acetate group is rather flexibly rotating with respect to the Rh-O bond along the reaction. In **10**, the distance between the acetate oxygen and hydrogen of phenyl group is very close, less than 2.1 Å. Next, proton transfer and Rh-C bond formation take place through transition state **TS$_{10–11}$** to afford **11**. The geometry of **TS$_{10–11}$** is a distorted 6-membered transition state, which is similar to **TS$_{2–3}$** in path I. After the formation of **11**, several paths are conceivable. One is a simple reductive elimination of rhodium catalyst with acetic acid, proceeding through the transition state **TS$_{11–12}$** to afford **12** + [CpRh(AcOH)]. Another reductive elimination path may be possible, in which a chloride anion in the system takes an active role in the process (Figure 3 bottom). First, the Cl^- ion is replaced with acetate group in **11** to produce **14**. On this substitution process, **13** was found as the intermediate. The reductive elimination occurs from **14** to form **12** + $[CpRhCl]^-$ through transition state **TS$_{14–12}$**. An additional path, in which the acetic acid dissociates from the rhodium center before the elimination, was also found. However, this path is ruled out because of unrealistic, high energy.

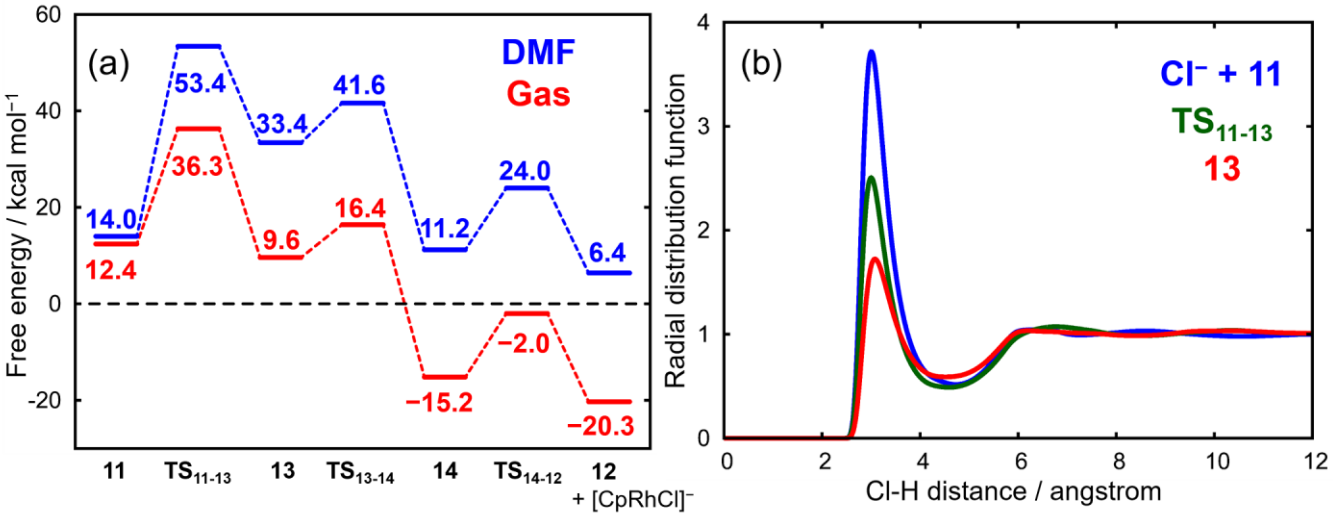

Figure 4. (a) Free energy changes along the reaction of path II with the ligand substitution in the gas phase (red line) and in DMF solution (blue line). (b) Radial distribution functions between the chloride and the hydrogen of DMF solvent for Cl^- (blue line), $TS_{11–13}$ (green line), and 13 (red line).

The free energy changes along the reaction of path II without the Cl^- substitution are shown in Figure 2 (right). In the gas phase, all the activation free energies of three transition states (**TS$_{1–10}$**, **TS$_{10–11}$** and **TS$_{11–12}$**) are about 20 kcal/mol. The situation is almost similar in DMF solution, and the rate determining

step is the rotation of pyrazole (**TS$_{1–10}$**) both in the gas phase (20.2 kcal/mol) and in DMF solution (22.9 kcal/mol). This indicates that the barrier of the Rh–N cleavage and the solvent coordination to rhodium may not be important in the selectivity, which may contradict our instinct. Instead, the stability of final product **12** in the gas phase are remarkably different from that in DMF solution. The reaction energy for the elimination with acetic acid is −5.9 kcal/mol in the gas phase whereas it is increased to 13.16 kcal/mol in DMF solution. Namely, the reaction of path II is exothermic only in the gas phase, suggesting that the generation of quinoline derivative is achieved only in *o*-xylene environment. The other path from **11** through the ligand substitution between the chloride anion and acetic acid is also examined (Figure 4a). However, the activation free energies of **TS$_{10–11}$** are considerably higher than those without the ligand substitution. Especially, that in DMF solution is increased to 53.4 kcal/mol. Therefore, the elimination step with chloride anion seems to be unrealistic in DMF solution.

Solvation free energy and solvation structure

Why **12** becomes unstable? To address this question, the solvation free energy $\Delta\mu$ is further analyzed. As shown in EXPERIMENTAL section, $\Delta\mu$ can be decomposed into the contribution from each atom $\Delta\mu_\alpha$. Then $\Delta\mu$ is represented as the sum of contributions from each moiety in the complex by summing over the corresponding indices α. Based on this quantity, $\Delta\mu$ were decomposed into the contributions from the quinoline moiety corresponding to **12** ($\Delta\mu_{\mathrm{Q}}$) and other part including Rh, AcOH and Cp ring ($\Delta\mu_{\mathrm{other}}$). We compared $\Delta\mu_{\mathrm{Q}}$ and $\Delta\mu_{\mathrm{other}}$ of **11** to those of **12** and CpRh(AcOH). Both of them are considerably destabilized. $\Delta\mu_{\mathrm{Q}}$ is changed from −27.0 to −19.1 kcal/mol, and $\Delta\mu_{\mathrm{other}}$ is changed from −25.0 to −13.5 kcal/mol. This is mainly attributed to the change in the electronic structure on the process. The total amount of Mulliken charges assigned on the quinoline moiety in **11** is about −0.37, which becomes zero in **12**. Therefore, the electrostatic stabilization between solute and solvent is weakened on the dissociation, and the solvation free energy is increased in the final step.

The RISM-SCF-SEDD method provides the solvation structure described as a set of radial distribution functions (RDFs). As reported in our previous study,[5] the solvent coordination to rhodium center after the cleavage of Rh-N coordination bond was not so significant. One of the remarkable changes in solvation structure is found around the chloride atom in path II with the ligand substitution. As the reaction proceeds from **11** associating with Cl^- to form **13**, The increase in $\Delta\mu$ is more than 20 kcal/mol. In particular, the increase in the chloride site, $\Delta\mu_{\mathrm{Cl}}$, is more than 40 kcal/mol, which is the main contribution of the destabilization in DMF solution. RDFs between chloride and hydrogen of DMF are

shown in Figure 4(b). The sharp peaks located around 3.0 Å are assigned to hydrogen bonding, whose heights are monotonically decreased from the isolated Cl^- to **13**. Absolute values of Cl charges are also decreased, and the charge is delocalized mainly to the cyclopentadienyl ligand.

CONCLUSION

We theoretically studied the reaction paths and solvation effects of rhodium-catalyzed oxidative coupling reaction by means of the RISM-SCF-SEDD method. It is a hybrid method of quantum chemistry and statistical mechanics, and the detailed information on solvation effect at the molecular level is available with medium computational cost.

The path for the naphthalene derivative, path I, is virtually independent of the reaction environment, and thus the naphthalene derivative can be produced both in *o*-xylene and DMF solution. In contrast, the reaction energy profiles for the quinoline derivative, path II, are significantly different between the gas phase and DMF solution. The reaction in the gas phase is exothermic whereas that in DMF solution is endothermic. These results are consistent with the experimental result. Therefore, the reaction energy in reductive elimination could become important to control the final product.

We would like to emphasize that the solvation effect on the chemical process including transition metal complex is not sufficiently understood although many experimental studies have been carried out in solution phase. A hybrid QM/MM type computation is required to address the present issue, but it is generally too time-consuming to treat the complex at a reasonably accurate level of theory. Because the RISM-SCF-SEDD is based on an analytical theory called integral equation theory for molecular liquid, the electronic structure described with high-level quantum chemical method is obtained together with information of solvation in molecular level. We believe that the RISM-SCF-SEDD is the only way to tackle the current topic at this moment. However, more accurate free energy evaluation could be desired to move toward a deeper understanding of the present process.

EXPERIMENTAL

Computational Procedure

Since the detailed explanations of the RISM-SCF and RISM-SCF-SEDD methods have been described elsewhere,[23] only the outline of the theory is presented here. Briefly, the solute electronic structure is calculated from solvated Fock operator including the averaged electrostatic potential arising from surrounding solvent molecules. The solvent distribution around a solute site is determined by the extended RISM theory, in which the solute-induced electrostatic potential field is incorporated. Both the

solute electronic structure and solvent distribution are simultaneously determined in a self-consistent manner. Hence the obtained wave function of the solute ($|\Psi_{\mathrm{sol}}\rangle$) is distorted (polarized) from the isolated one ($|\Psi\rangle$). Within the framework of RISM-SCF, the free energy of solution system is obtained by

$$A = E_{\mathrm{sol}} + \Delta\mu \,, \tag{1}$$

where E_{sol} is the total energy of the solute molecule, which is different from that of the isolated state (E_{isolated}). Using the standard electronic Hamiltonian of the solute $\hat{H}$,

$$\Delta E_{\mathrm{reorg}} = E_{\mathrm{sol}} - E_{\mathrm{isolated}} = \langle \Psi_{\mathrm{sol}} | \hat{H} | \Psi_{\mathrm{sol}} \rangle - \langle \Psi | \hat{H} | \Psi \rangle \tag{2}$$

represents the polarization of the solute molecule. $\Delta\mu$ is the solvation free energy. Several formulas with different approximations are available for $\Delta\mu$. In this study, the following well-known Gaussian fluctuation (GF) formula was adopted,

$$\Delta\mu = -\frac{\rho}{\beta} \sum_{\alpha}^{\text{solute}} \sum_{s}^{\text{solvent}} \int d\mathbf{r} \left\{ c_{\alpha s}(r) + \frac{1}{2} h_{\alpha s}(r) c_{\alpha s}(r) \right\}, \tag{3}$$

where $h_{\alpha s}(r)$ and $c_{\alpha s}(r)$ are the total and direct correlation function, ρ is the density of solvent and $\beta = 1/k_B T$. The subscript α refers to the interaction sites of solute molecules, and s refers to the sites on the solvent. $h_{\alpha s}(r)$ and $c_{\alpha s}(r)$ are obtained by solving the RISM equation, and the former is equivalent to the radial distribution function (RDF), $g_{\alpha s}(r)\left[\equiv h_{\alpha s}(r)+1\right]$. It is noted that the GF formula generally reproduces the experimental hydration free energies well compared with the other ones, such as the hyper-netted chain (HNC) formula. Actually, it was found that the free energy profile of the target system in DMF solution calculated with the HNC formula is rather similar to that in the gas phase, which makes it difficult to explain the solvent dependency. Therefore, we adopted the GF formula in the present study. $\Delta\mu$ given by Eq. (3) is formally divided into the contribution from each atom labeled α,

$$\Delta\mu_{\alpha} = -\frac{\rho}{\beta} \sum_{s}^{\text{solvent}} \int d\mathbf{r} \left\{ c_{\alpha s}(r) + \frac{1}{2} h_{\alpha s}(r) c_{\alpha s}(r) \right\}. \tag{4}$$

The quantity is useful to know how much each site contributes to total solvation free energy. It is noted that $\Delta\mu_{\alpha}$ is not the same as the solvation free energy of an atom α isolated in the solvent because the correlation functions in $\Delta\mu_{\alpha}$ also depend on the other atoms in the solute.

Computational Details

In the computations of DMF solution, the solvent density was set to be 0.93 g/cm^3 = 0.007663 molecule/Å^3, and temperature was set to be 353.15 K, which was the same as the experimental condition.

The RISM equation was solved with the HNC closure. The Lennard-Jones parameters were taken from previous studies[20,24–26] (Table 1). Unfortunately, direct computation of the *o*-xylene system with the RISM-SCF-SEDD method was extremely difficult because of a convergence problem in the RISM procedure. Since *o*-xylene was a typical non-polar solvent (relative permittivity $\varepsilon_r = 2.6$), the reaction in the gas phase was analyzed instead of the *o*-xylene system. Density functional theory with B3LYP functional[27] was used for the quantum chemical part of the computations throughout the study. The core electrons of Rh (up to 4f) were replaced with effective core potential (ECP) of Stuttgart group, and associated basis sets was employed for valence electrons.[28] We employed the 6-31G(d) basis set for H, C, N, and O atoms, and the 6-31+G(d) basis set for Cl atom.[29] All the geometry optimization in the gas phase was performed with Gaussian16 program package.[30] The thermal corrections to free energies were obtained at 353.15 K from the frequency calculations. The free energies in DMF solution were then calculated using the geometries optimized in the gas phase with GAMESS program package,[31] where we implemented the RISM-SCF-SEDD routine.

Table 1. Lennard-Jones parameters for solute and solvent

Molecule	Site	σ/Å	ε/kcal mol^{-1}	q/|e|[a]
Solute	Rh	4.68	0.053	-
	C	3.75	0.105	-
	N	3.25	0.170	-
	O	2.96	0.210	-
	H	1.07	0.055	-
	Cl	3.62	0.448	-
DMF	N	3.25	0.140	−0.570
	C	3.75	0.105	0.340
	Me	3.80	0.130	0.285
	O	2.96	0.210	−0.460
	H	2.75	0.038	0.120

[a] Note that the electronic structure of the solute is determined in a self-consistent manner.

ACKNOWLEDGEMENTS

The authors gratefully acknowledge the valuable comments and suggestions made by Prof. Shigeyoshi Sakaki and Dr. Yu-ya Ohnishi. The work is financially supported by JSPS KAKENHI (Grant Nos. JP17H03009, JP17H06092, JP20H04813, and JP20H05839). Theoretical computations were partly performed using Research Center for Computational Science, Okazaki, Japan.

REFERENCES AND NOTES

1. J. E. Anthony, *Angew. Chem. Int. Ed.*, 2008, **47**, 452.
2. T. Takahashi, M. Kitamura, B. Shen, and K. Nakajima, *J. Am. Chem. Soc.*, 2000, **122**, 12876.
3. N. Umeda, H. Tsurugi, T. Satoh, and M. Miura, *Angew. Chem. Int. Ed.*, 2008, **47**, 4019.
4. T. Fukutani, K. Hirano, T. Satoh, and M. Miura, *Org. Lett.*, 2009, **11**, 5198; T. Fukutani, K. Hirano, T. Satoh, and M. Miura, *J. Org. Chem.*, 2011, **76**, 2867.
5. N. Umeda, K. Hirano, T. Satoh, N. Shibata, H. Sato, and M. Miura, *J. Org. Chem.*, 2011, **76**, 13.
6. D. L. Davies, S. M. A. Donald, O. Al-Duaij, S. A. Macgregor, and M. Polleth, *J. Am. Chem. Soc.*, 2006, **128**, 4210; Y. Boutadla, D. L. Davies, R. C. Jones, and K. Singh, *Chem. Eur. J.*, 2011, **17**, 3438; Y. Boutadla, D. L. Davies, O. Al-Duaij, J. Fawcett, R. C. Jones, and K. Singh, *Dalton Trans.*, 2010, **39**, 10447.
7. L. Li, Y. Jiao, W. W. Brennessel, and W. D. Jones, *Organometallics*, 2010, **29**, 4593.
8. L. Li, W. W. Brennessel, and W. D. Jones, *Organometallics*, 2009, **28**, 3492.
9. L. Li, W. W. Brennessel, and W. D. Jones, *J. Am. Chem. Soc.*, 2008, **130**, 12414.
10. T. K. Hyster and T. Rovis, *J. Am. Chem. Soc.*, 2010, **132**, 10565.
11. S. Ten-no, F. Hirata, and S. Kato, *J. Chem. Phys.*, 1994, **100**, 7443.
12. H. Sato, F. Hirata, and S. Kato, *J. Chem. Phys.*, 1996, **105**, 1546.
13. D. Yokogawa, H. Sato, and S. Sakaki, *J. Chem. Phys.*, 2007, **126**, 244504.
14. D. Chandler and H. C. Andersen, *J. Chem. Phys.*, 1972, **57**, 1930.
15. F. Hirata and P. J. Rossky, *Chem. Phys. Lett.*, 1981, **83**, 329.
16. K. Iida, D. Yokogawa, H. Sato, and S. Sakaki, *Chem. Phys. Lett.*, 2007, **443**, 264; K. Iida, D. Yokogawa, A. Ikeda, H. Sato, and S. Sakaki, *Phys. Chem. Chem. Phys.*, 2010, **11**, 8556.
17. S. Hayaki, D. Yokogawa, H. Sato, and S. Sakaki, *Chem. Phys. Lett.*, 2008, **458**, 329; H. Sato, C. Kikumori, and S. Sakaki, *Phys. Chem. Chem. Phys.*, 2011, **13**, 309; M. Higashi and S. Kato, *J. Phys. Chem. A*, 2005, **109**, 9867.
18. S. Hayaki, K. Kido, H. Sato, and S. Sakaki, *Phys. Chem. Chem. Phys.*, 2010, **12**, 1822; S. Hayaki, K. Kido, D. Yokogawa, H. Sato, and S. Sakaki, *J. Phys. Chem. B*, 2009, **113**, 8227.
19. J. Tomasi, B. Mennucci, and R. Cammi, *Chem. Rev.*, 2005, **105**, 2999.
20. H. Sato and F. Hirata, *J. Phys. Chem. A*, 2002, **106**, 2300.
21. H. Sato, I. Kawamoto, D. Yokogawa, and S. Sakaki, *J. Mol. Liq.*, 2007, **136**, 194.
22. Temperature in the previous study[5] was set to 298.15 K.
23. 'Molecular Theory of Solvation,' ed. by F. Hirata, Kluwer, Dordrecht, 2003.; 'Continuum Solvation Models in Chemical Physics: From Theory to Applications,' ed. by B. Mennucci and R. Cammi, Wiley, New York, 2007.

24. W. L. Jorgensen and C. J. Swenson, *J. Am. Chem. Soc.*, 1985, **107**, 569.
25. A. K. Rappe, C. J. Casewit, K. S. Colwell, W. A. Goddard III, and W. M. Skiff, *J. Am. Chem. Soc.*, 1992, **114**, 10024.
26. H. Sato and F. Hirata, *J. Am. Chem. Soc.*, 1999, **121**, 3460.
27. A. D. Becke, *J. Chem. Phys.*, 1993, **98**, 5648; P. J. Stephens, F. J. Devlin, C. F. Chablowski, and M. J. Frisch, *J. Phys. Chem.*, 1994, **98**, 11623.
28. D. Andrae, U. Haussermann, M. Dolg, H. Stoll, and H. Preuss, *Theor. Chim. Acta*, 1990, **77**, 123.
29. W. J. Hehre, R. Ditchfield, and J. A. Pople, *J. Chem. Phys.*, 1972, **56**, 2257.
30. M. J. Frisch, G. W. Trucks, H. B. Schlegel, G. E. Scuseria, M. A. Robb, J. R. Cheeseman, G. Scalmani, V. Barone, G. A. Petersson, H. Nakatsuji, X. Li, M. Caricato, A. V. Marenich, J. Bloino, B. G. Janesko, R. Gomperts, B. Mennucci, H. P. Hratchian, J. V. Ortiz, A. F. Izmaylov, J. L. Sonnenberg, D. Williams-Young, F. Ding, F. Lipparini, F. Egidi, J. Goings, B. Peng, A. Petrone, T. Henderson, D. Ranasinghe, V. G. Zakrzewski, J. Gao, N. Rega, G. Zheng, W. Liang, M. Hada, M. Ehara, K. Toyota, R. Fukuda, J. Hasegawa, M. Ishida, T. Nakajima, Y. Honda, O. Kitao, H. Nakai, T. Vreven, K. Throssell, J. A. Montgomery, Jr., J. E. Peralta, F. Ogliaro, M. J. Bearpark, J. J. Heyd, E. N. Brothers, K. N. Kudin, V. N. Staroverov, T. A. Keith, R. Kobayashi, J. Normand, K. Raghavachari, A. P. Rendell, J. C. Burant, S. S. Iyengar, J. Tomasi, M. Cossi, J. M. Millam, M. Klene, C. Adamo, R. Cammi, J. W. Ochterski, R. L. Martin, K. Morokuma, O. Farkas, J. B. Foresman, and D. J. Fox, Gaussian 16, Revision A.03, Gaussian Inc., Wallingford CT, 2016.
31. M. W. Schmidt, K. K. Baldridge, J. A. Boatz, S. T. Elbert, M. S. Gordon, J. H. Jensen, S. Koseki, N. Matsunaga, K. A. Nguyen, S. J. Su, T. L. Windus, M. Dupuis, and J. A. Montgomery, *J. Comput. Chem.*, 1993, **14**, 1347.